15

NASA
Technical
Paper
2285

February 1984

Beam Impingement Angle Effects on Secondary Electron Emission Characteristics of Textured Pyrolytic Graphite

Arthur N. Curren
and Kenneth A. Jensen

NASA

NASA Technical Paper 2285

1984

Beam Impingement Angle Effects on Secondary Electron Emission Characteristics of Textured Pyrolytic Graphite

Arthur N. Curren
and Kenneth A. Jensen

Lewis Research Center
Cleveland, Ohio

NASA
National Aeronautics
and Space Administration

Scientific and Technical Information Branch

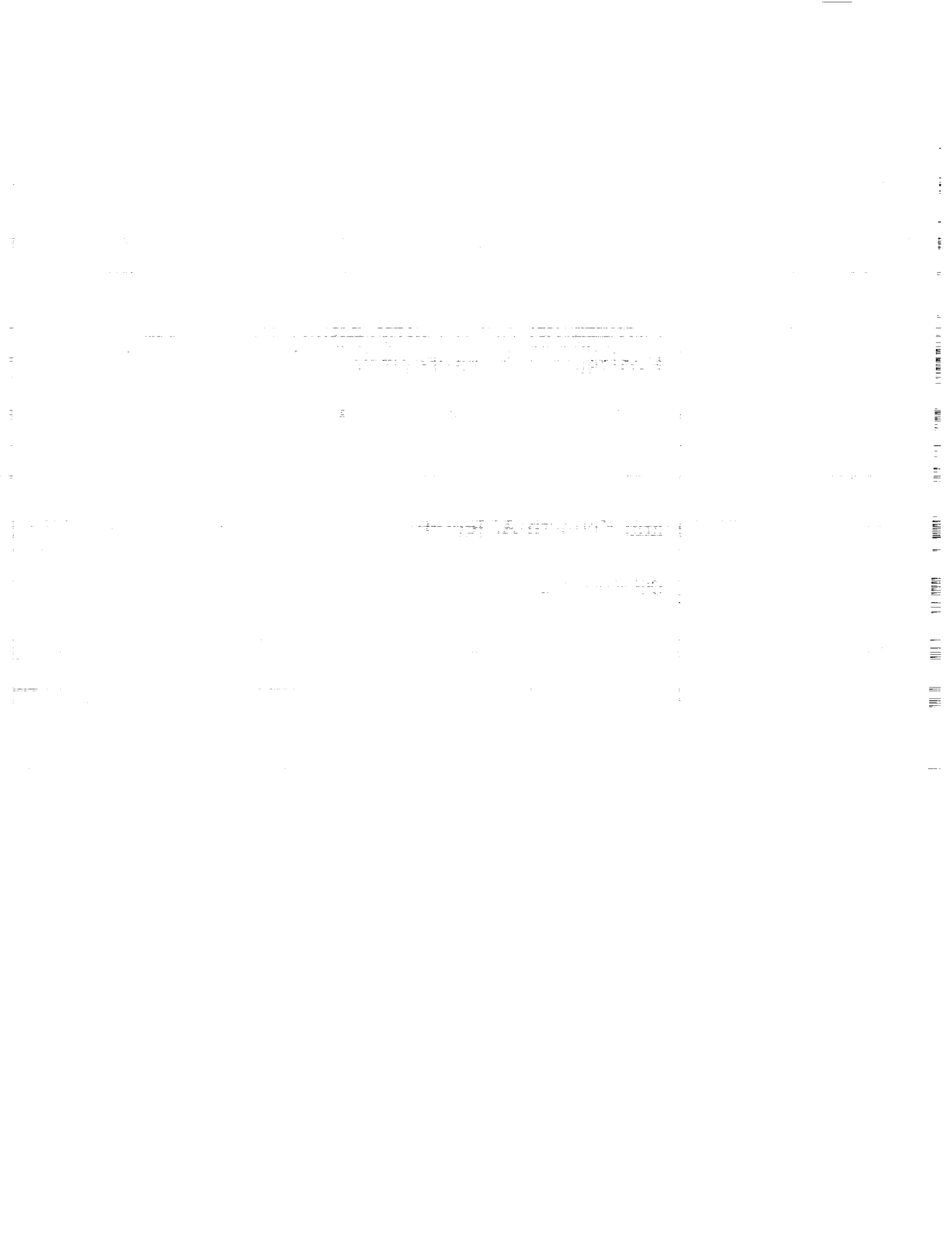

Summary

Experimentally determined values of true secondary electron emission and relative values of reflected primary electron yield for untreated and ion-textured pyrolytic graphite over a range of primary electron energy levels and electron beam impingement angles are presented. The purpose of the investigation is to provide information required to develop high-efficiency multistage depressed collectors (MDC's) for microwave amplifier traveling-wave tubes for space communication and aircraft applications. To attain the highest possible MDC efficiencies, the electrode surfaces must have low secondary electron emission characteristics. Pyrolytic graphite, a chemically vapor-deposited material, is a particularly promising candidate for this application.

The pyrolytic graphite surfaces studied in this investigation were tested over a range of primary electron beam energies and beam impingement angles from 200 to 2000 eV and direct (0°) to near-grazing angles (85°), respectively. Surfaces both parallel to and normal to the planes of material deposition were examined. The true secondary electron emission and reflected primary electron yield characteristics of the pyrolytic graphite surfaces are compared to those of sooted control surfaces. While soot, or carbon black, is not suitable for MDC use, it provides a consistently reproducible *ideal* comparison surface because of its known extremely low secondary electron emission characteristics. The ion-textured pyrolytic graphite surfaces which were studied exhibited extremely low true secondary electron emission and reflected primary electron yield characteristics, even lower than those of the sooted surfaces at small electron beam impingement angles.

Introduction

Improving the overall efficiency of microwave amplifier traveling-wave tubes (TWT's) has been an ongoing effort at the NASA Lewis Research Center. Because of the limited electrical power available to operate these tubes in space communication and to some extent in aircraft applications, the need for high efficiency to provide high radiofrequency (rf) output power is evident. The increased efficiency may be reflected in smaller and lighter power supplies, lower heat rejection rates, larger spacecraft and aircraft payloads, and other dividends associated with the use of high-efficiency components.

The invention and development of the multistage depressed collector (MDC) have resulted in a significant increase in collector efficiency (ref. 1) and, consequently overall TWT electrical efficiency. After the spent electron beam passes through the TWT's interaction section, it is slowed in the MDC by a retarding electrical field, and the electrons impinge the electrodes at reduced energies. To usefully recover the maximum kinetic energy in the electron beam and thereafter achieve high collector efficiency, the electrode surfaces must have low secondary electron emission characteristics (ref. 2) so that the electrons are not excessively reflected or reemitted from the collector. A number of methods have been used to provide relatively low secondary electron emission electrode surfaces for MDC's, including coating the surfaces with materials known to have lower secondary electron emission characteristics than do the electrode materials themselves. One example of this method which has been used is titanium carbide sputter applied to copper electrodes.

Pyrolytic graphite, a mechanically strong, high-temperature anisotropic material which has a low vapor pressure, high thermal emissivity, and high planar thermal conductivity (ref. 3), is a promising candiate for the MDC electrode application. It has been demonstrated that the already low secondary electron emission characteristics of this material can be reduced even further by appropriately texturing the surface (ref. 4), and more recent studies have further identified the effects of ion-beam texturing of pyrolytic graphite (ref. 5). Specifically, pyrolytic graphite samples which have been subjected to certain ion-texturing procedures have exhibited lower secondary electron emission characteristics than those for untreated surfaces of the same material, and they have exhibited significantly lower emission characteristics than those of customary electrode materials such as copper.

Analytical studies of the MDC charge trajectories (ref. 6) indicate that the electrons impinge the electrodes at various angles, ranging from direct impingement (0° from normal to the surface) to near-grazing angles. Therefore, to properly assess the effectiveness of any proposed MDC electrode material relative to other candidates, it is necessary to have a good knowledge of its secondary electron emission characteristics over a representative range of electron beam impingement angles as well as over a wide range of primary electron beam energy levels. The material presented in this report is intended to contribute to that knowledge for untreated and ion-textured pyrolytic graphite.

Background Information

TWT and MDC Considerations

High-efficiency microwave amplifier TWT's use MDC's. The magnetic field which confines the electron beam in the rf interaction section of the TWT is removed at the MDC entry port, from which point the beam diverges and the electrons are slowed by a retarding

electrical field to be collected selectively by electron energies with relatively small losses. The MDC efficiency is directly influenced by the ability of the electrodes to absorb and retain the impinging electrons. To attain the highest efficiency, the electrodes must have a low secondary electron emission ratio, or ratio of reemitted electrons to impinging electrons.

Secondary Electron Emission as an MDC Loss Mechanism

Secondary electron emission occurs when electrons bombard a solid surface. It consists of electrons which undergo inelastic collisions at or near a surface and are emitted at a few tens of electron volts (true secondary electron emission), electrons which experience elastic collisions with little or no energy loss and leave the surface at or very near the primary beam energy level (reflected primary electron yield), and other electrons which suffer some inelastic collisions and are reemitted at intermediate energy levels (rediffused electron emission). True secondary electron emission and reflected primary electron yield are indicated by large peaks on the energy distribution curve for a conducting material. For materials with low atomic number (such as carbon) and for primary electron beam energies less than several kilovolts, reflected primary electron yield and rediffused electron emission are considered to be a small fraction of the total number of secondary electrons emitted. Consequently, for these cases, only a small error is made in assuming total secondary electron emission is approximated by true secondary electron emission (refs. 4, 7, and 8). For this study, the true secondary electron emission and reflected primary electron yield characteristics of pyrolytic graphite will be examined as functions of primary electron beam energy level and beam impingement angle.

Figure 1 is a simplified representation of an MDC section illustrating typical electrode voltages, where $-V_0$ is the cathode potential. Electrons having the highest energy will impinge electrode 4, while those electrons having less energy will be collected on the lower numbered electrodes. While most of the electrons are collected on the top surfaces of the electrodes, some strike the bottom surfaces. True secondary electrons that come off the top of the collector electrodes are retarded by the electric field and return to their respective electrodes with only small energy losses, while true secondaries and reflected primary electrons which reemit from the bottom electrode surfaces are accelerated by the electric field and are collected on lower electrodes with larger energy losses, resulting in a decrease in MDC efficiency. If reflected primary electrons are emitted from the top surfaces of the electrodes, they may have energies high enough to escape the confining electric field and be in an accelerating field, with additional significant energy losses. While it is apparent that both true secondary and reflected primary electron emission are undesirable and should be reduced to a minimum, reflected primary electron yield represents a larger loss mechanism per electron than true secondary electron emission. This description of MDC loss mechanism due to secondary electron emission is treated further in reference 4.

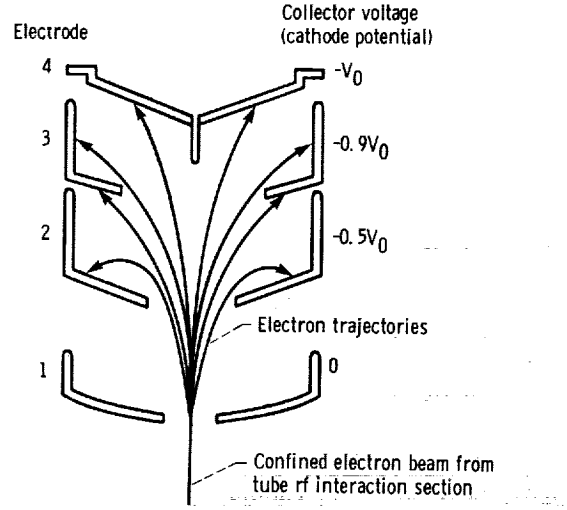

Figure 1. – Schematic multistage depressed collector configuration for a traveling-wave tube.

Pyrolytic Graphite as an MDC Electrode Material

As stated earlier, pyrolytic graphite[1], a strong, lightweight material which has been shown to have relatively low secondary electron emission characteristics (ref. 4) is particularly well-suited for the MDC electrode application. Also, pyrolytic graphite has low vapor pressure, high thermal emissivity, high thermal conductivity in the plane of material deposition, and very high allowable operating temperature (ref. 3), all of which permit effective thermal control and high power density operation. It is a chemically vapor-deposited material which is formed in a low-pressure, highly carbonaceous atmosphere by the thermal cracking of a hydrocarbon source gas such as natural gas, methane, or propane. The deposition process takes place at temperatures from about 1500° to 2500° C or higher, and the product generally is formed on mandrels of a suitable high-temperature material such as carbon. The material is anisotropic, with most of the properties measured in the AB direction (parallel to the plane of material deposition) being significantly different from those measured in the C direction (perpendicular to the plane of deposition). Table I presents for comparison some of

[1]The material referred to in this investigation as pyrolytic graphite is also referred to by some as pyrolytic carbon (ref. 9) to distinguish it from a more highly oriented graphite product formed by severe thermal or stress annealing. The term pyrolytic graphite is used extensively to describe the material used in this study and is now generally accepted.

TABLE I. – SOME SELECTED PROPERTIES OF PYROLYTIC GRAPHITE, OFHC COPPER, AND MOLYBDENUM

Property	Smooth pyrolytic graphite		OFHC copper	Molybdenum
	AB direction	C direction		
Density at room temperature, g/cm^3	2.20	2.20	8.94	10.20
Sublimation/melting temperature, °C	3 650	3 650	1 083	2 620
Total normal thermal emissivity	[a]0.78	[a]0.49	[b]0.023	[b]0.08
Tensile strength, Pa (psi):				
At room temperature	9.65×10^7 (14 000)	2.76×10^6 (400)	1.93×10^8 (28 000)	6.55×10^8 (~95 000)
At 2204° C	1.38×10^8 (20 000)	1.03×10^6 (150)	0	~0
Compressive strength, Pa (psi):				
At room temperature	6.89×10^7 (10 000)	3.10×10^8 (45 000)	-----	-----
At 2204° C	7.58×10^7 (11 000)	4.14×10^8 (60 000)	0	~0
Thermal conductivity at room temperature, cal/cm^2/cm/sec/°C	0.827	0.004	0.934	0.3
Modulus of elasticity, Pa (psi):				
At room temperature	2.76×10^{10} (4×10^6)	2.76×10^{10} (4×10^6)	1.10×10^{11} (16×10^6)	3.24×10^{11} (47×10^6)
At 2204° C	1.72×10^{10} (2.5×10^6)	1.72×10^{10} (2.5×10^6)	0	~0

[a]At 980° C.

[b]At room temperature.

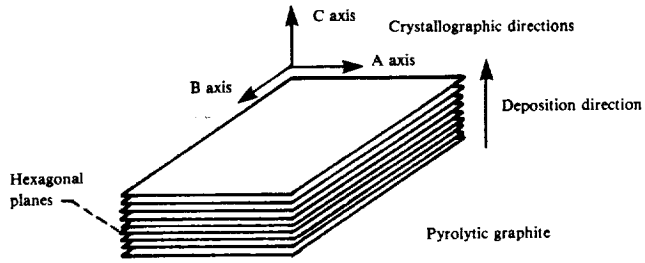

the properties of pyrolytic graphite and those of some conventional MDC electrode materials such as oxygen-free, high-conductivity (OFHC) copper and molybdenum. Pyrolytic graphite has adequate mechanical strength and stiffness, and it has a definite density and thermal emissivity advantage over the other materials noted. Thermal conductivity in the AB direction very nearly equals that of OFHC copper and is much higher than that of molybdenum. The property values listed in table I are from references 3 and 8. Currently, the major producers of pyrolytic graphite in the United States include the B. F. Goodrich Company, Super-Temp Operations, of Santa Fe Springs, California, Pfizer, Inc., Minerals, Pigments and Metals Division, of Easton, Pennsylvania, and the Union Carbide Corporation, Carbon Products Division, of Cleveland, Ohio. Samples of pyrolytic graphite from the regular product line of each of these suppliers were obtained and included in this investigation. Product information from each of the listed suppliers is presented in references 10, 11, and 12, respectively.

Data in reference 4 indicate that the already low secondary electron emission characteristics of pyrolytic graphite can be reduced even further by appropriately ion-texturing the surface. The resulting textured surface is characterized by a dense array of relatively uniformly sized spires or cones, the spacing and height of which are in the range of a few micrometers. More recent studies (ref. 5) have further examined the effects of ion-texturing processes on the secondary electron emission characteristics of this material, and an experimental investigation was conducted (ref. 13) which verified the potential for TWT overall efficiency improvement with the use of ion-textured pyrolytic graphite.

The data presented in this report expand the existing information relative to the use of ion-textured pyrolytic graphite as an MDC electrode material by relating the secondary electron emission characteristics to the primary electron beam energy level and beam impingement angle.

Apparatus and Equipment

Ion-Texturing Facility

A schematic of the facility used for ion-texturing the pyrolytic graphite surfaces studied in this investigation is presented in figure 2. The vertically mounted cylindrical plasma chamber (approx 38 cm (15 in.) outside diameter by 24 cm (9.5 in.) high) is a 30-cm argon ion source which was modified from a previous use (ref. 14). The plasma chamber utilizes a hollow cathode which includes a

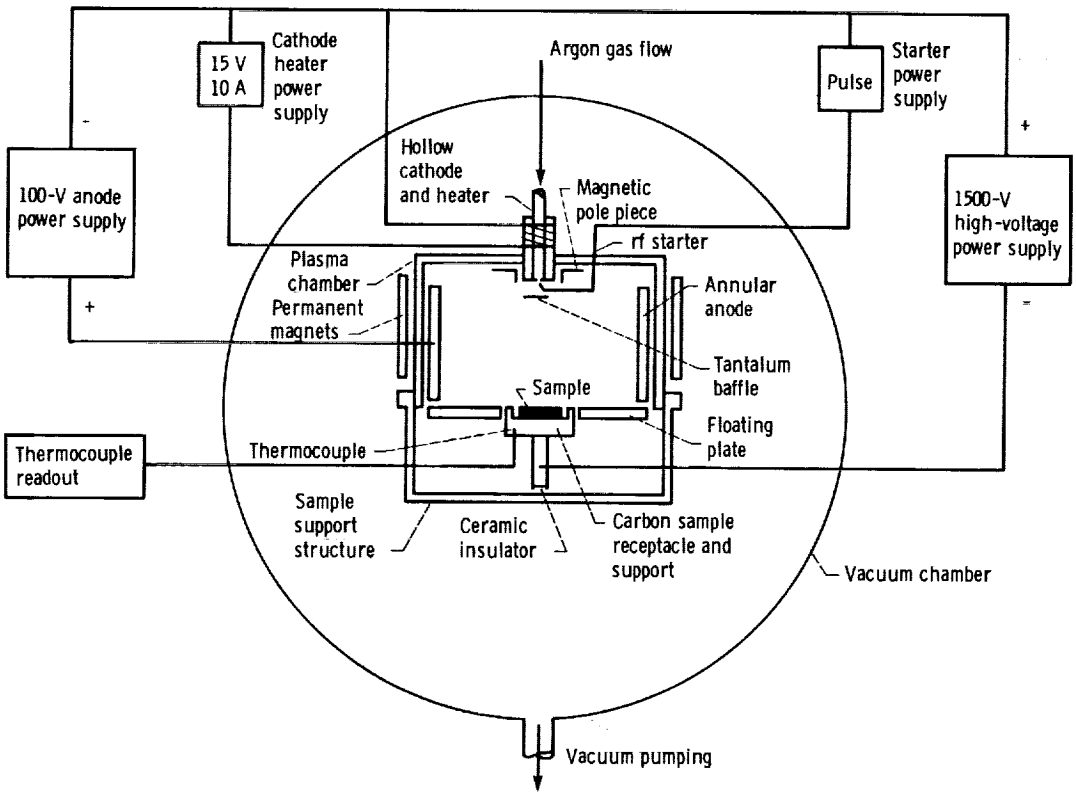

Figure 2. – Schematic of ion-texturing apparatus.

porous tungsten cylindrical insert impregnated with barium oxide as a dispenser of low work function material. Argon gas is passed through the hollow cathode and into the chamber through a 0.076-cm- (0.030-in.-) diameter orifice. Plasma discharge is initiated by applying a brief 3-kV pulse to a probe located 0.2 cm (0.079 in.) from the cathode tip. Details of the pulse starting procedure are included in reference 14. The pyrolytic graphite samples which were textured were disks approximately 2.1 cm (0.838 in.) in diameter and 0.15 cm (0.060 in.) thick. Before texturing, the disks were cleaned by successively wiping them with clean acetone and high-purity ethyl alcohol, using a clean lint-free cloth or absorbant paper. The samples were positioned in a carbon receptacle as indicated in figure 2 and shown in the photograph in figure 3(a). The sample support receptacle is instrumented with thermocouples to monitor the sample temperature during texturing. An electrically floating solid plate surrounds the receptacle and restricts the plasma to the sample location.

The large vacuum chamber in which the plasma chamber is operated is about 91.5 cm (3 ft) in diameter and about 61 cm (2 ft) long. It is equipped with pumps of such capacity that a pressure of about 1.33×10^{-4} Pa (1×10^{-6} torr) can be maintained with no argon gas flow and pressures from about 2.66×10^{-3} to 7.98×10^{-3} Pa (2×10^{-5} to 6×10^{-5} torr) can be maintained when argon gas is being introduced into the plasma chamber. The plasma chamber is attached to the removable door of the vacuum chamber as shown in the photograph in figure 3(b) for ease of access to the equipment. The chamber door is fitted with appropriate vacuum feedthrough devices to accommodate the instrumentation and electrical leads and gas lines indicated in figure 2.

A brief description of the operating procedure used for this investigation is as follows (see also fig. 2). After the material sample to be textured and the sample support receptacle are positioned, the vacuum chamber is closed, sealed, and pumped to about 1.33×10^{-4} Pa (1×10^{-6} torr). Argon is ducted into the plasma chamber through the hollow cathode at a rate of about 50 to 70 standard cm^3/min, and the cathode heater power and anode power are applied. After the cathode reaches its operating temperature, ion discharge is established by activating briefly the high-voltage pulser. Ion bombardment of the sample surface is then started by activating the high-voltage power supply to establish a potential difference between the plasma and the sample. The sample surface current density is determined by dividing the high-voltage power supply current by the area of the carbon sample receptacle exposed to the plasma. This current is adjustable over a range adequate to provide the sample surface current densities for the samples reported in this study. After texturing begins, the various operating parameters may be adjusted to provide the desired sample surface current density and to ensure operating

(a) Sample support receptacle and structure with pyrolytic graphite sample in position prior to installation in ion-texturing apparatus.
(b) Ion-texturing apparatus showing sample support structure and receptacle in position.

Figure 3. – Positioning of samples for ion-texturing.

stability. The argon flow rate is commonly reduced to about one-half the starting level, and the cathode heater power may be reduced significantly. The length of time the texturing continues is, of course, at the option of the operator.

Testing Facility

The apparatus used for measuring the secondary electron emission characteristics of the materials studied in this investigation is shown schematically in figure 4. The sample disk to be tested is held vertically (on a diameter) in a micromanipulator-mounted fixture inside an ultra-high vacuum chamber which is fitted with an Auger spectrometer cylindrical mirror analyzer (CMA), a residual gas analyzer (RGA), vacuum feedthrough fittings, and other appropriate equipment. A filament heater/reflector system and thermocouple are incorporated into the sample-holding fixture for sample degassing and temperature monitoring. The vacuum chamber is capable of being pumped to a pressure of 1.33×10^{-8} Pa (1×10^{-10} torr) or lower, and the micromanipulator can translate the sample short distances (12.5 mm in two directions on the horizontal plane and 40 mm vertically) and rotate the sample about its vertical axis 90° in either direction. Supporting external equipment includes a scanning electron microscope for sample surface examination, appropriate power supplies, and switching and sensor readout devices for sample biasing and to perform the required measurements.

With the sample installed in the holding fixture and the vacuum chamber closed and sealed, the procedures preparatory to sample testing begin with pumping to the operating pressure of 1.33×10^{-8} Pa (1×10^{-10} torr). During this pumping process, a *clamshell* heater/cover is placed over the vacuum chamber and the chamber is heated to about 250° C for 16 hours to degas the system. Following this procedure, the sample is heated by filament radiation and electron bombardment to about 500° C for 3 to 4 hours to degas the sample and simulate the anticipated bakeout temperature to which an MDC assembly on a TWT would be subjected. During this bakeout period, the RGA typically indicates a rapid reduction of gas from the sample to insignificant levels.

Auger examinations of the sample surfaces and

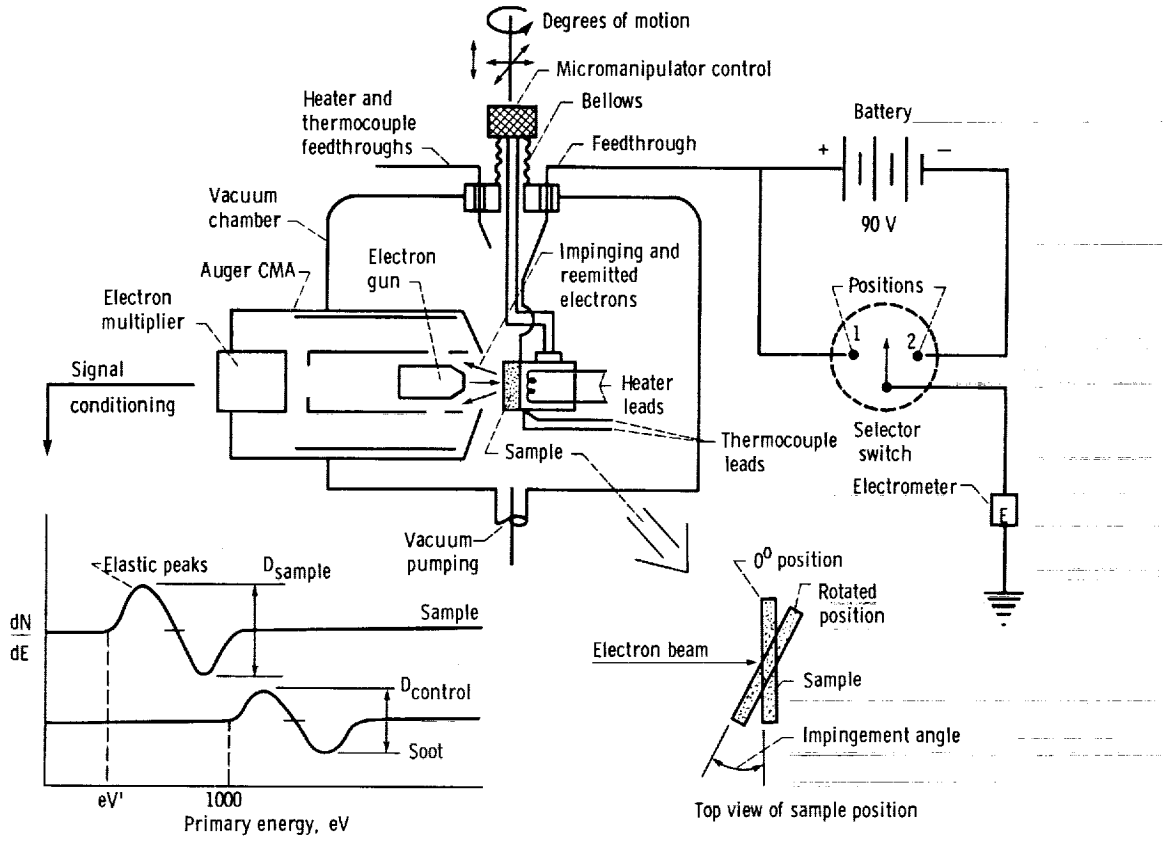

Figure 4. – Schematic of experimental apparatus used for measuring secondary electron emission. Not shown are vacuum chamber ports for viewing, residual gas analyzer, and other uses.

secondary electron emission measurements were conducted after the described 16-hour bakeout period, and then again after the 500° C bakeout. These examinations and measurements are discussed in detail later in this report.

Experimental and Calculation Procedures

Surfaces Investigated

Scanning electron microscope photomicrographs of the surfaces studied in this investigation are presented in figures 5(a) to (e). The surface shown in figure 5(a) is the control or comparison surface which was formed by coating an untreated pyrolytic graphite surface with soot or carbon black by means of a fuel-rich oxy-acetylene torch. The photomicrograph indicates a relatively smooth surface composed of many small particles of uniform size and having no major or outstanding projections. An untreated pyrolytic graphite AB surface is shown in the photomicrograph of figure 5(b). Although this surface has no major projections, it is characterized by randomly occurring minor depressions and raised areas with some scattered features which resemble small particles of debris but which are firmly attached to the surface. The surface characteristics shown in figure 5(c) are created when an untreated pyrolytic graphite AB surface is ion-textured using the parameters indicated in the figure. The dense random array of spires extends perpendicularly from the surface to an average height of 4 to 5 μm with an average spacing of 2 to 3 μm. A typical untreated pyrolytic graphite C surface is shown in figure 5(d). This surface is quite different from the relatively smooth untreated AB surface, since it is characterized by closely arrayed but nonuniform and shallow (1 to 2 μm) depressions separated by ridges. Since the ridges appear to be oriented in one general direction, it is assumed that they are parallel to the plane of material deposition. When the untreated C surface is ion-textured according to the parameters indicated in figure 5(e), the surface shown in the photomicrograph (fig. 5(e)) is developed. This surface displays an extremely closely arrayed pattern of spires averaging 5 to 6 μm in height and 1 to 2 μm apart. It differs from the ion-textured AB surface (fig. 5(c)) in that the ion-textured C surface shows significantly more uniform spire size and closer and more uniform spire spacing. Extensive experience with the texturing process at Lewis indicates that the differences in the physical characteristics between the ion-textured AB and C surfaces were not a result of the small differences

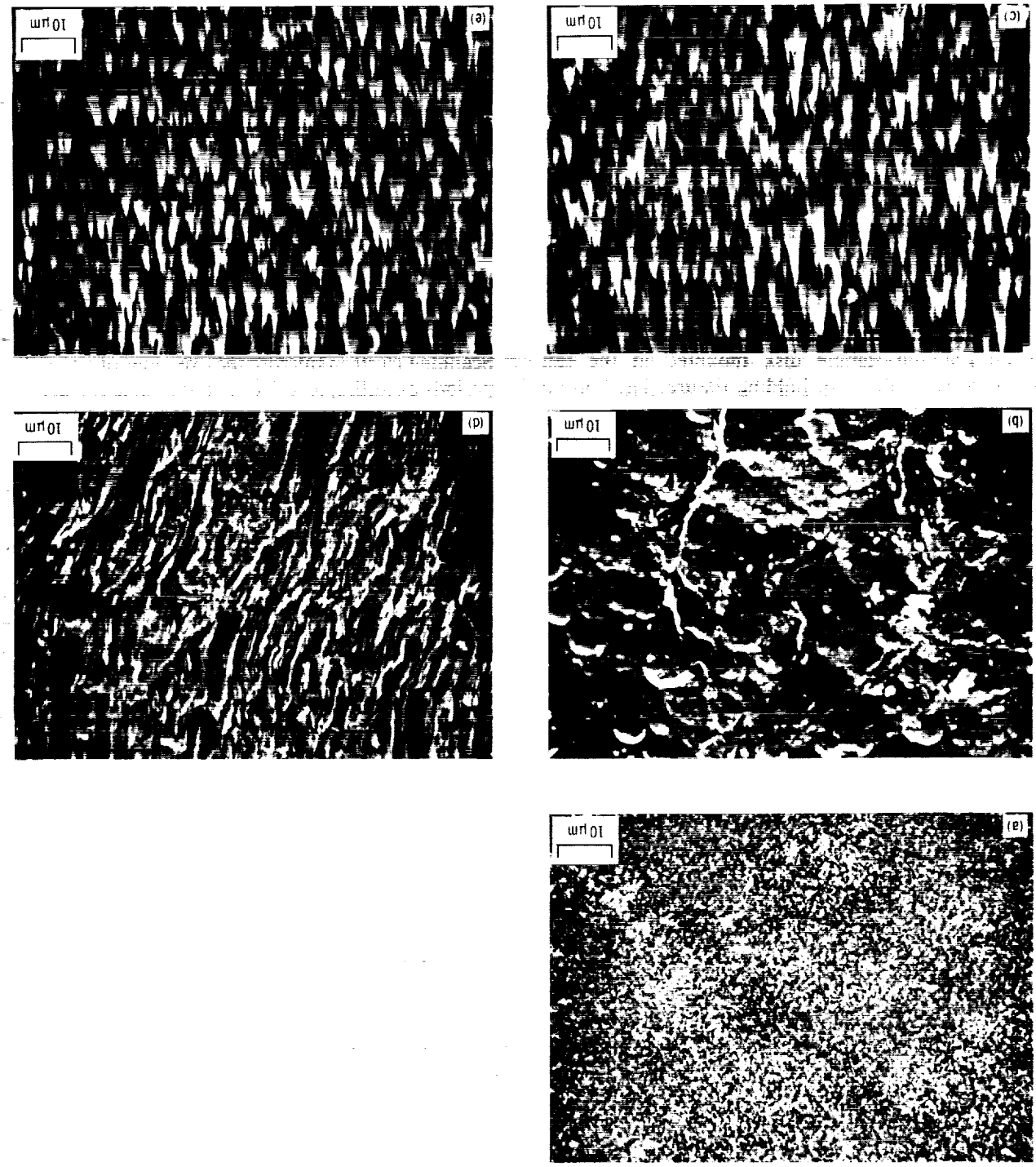

(a) Soot on smooth, untreated pyrolytic graphite AB surface.
(b) Smooth, untreated pyrolytic graphite AB surface.
(c) Ion-textured pyroyltic graphite AB surface. Texturing parameters: Surface current density, 4.5 mA/cm^2; accelerating potential, 1100 V dc; texturing period, 4 hr; argon flow rate, 34 sccm; vacuum chamber pressure, $\sim 1.2 \times 10^{-3}$ Pa (9×10^{-6} torr); temperature (sample receptacle average), 520° C.
(d) Untreated pyrolytic graphite C surface.
(e) Ion-textured pyrolytic graphite C surface. Texturing parameters: surface current density, 5 mA/cm^2; accelerating potential, 1000 V dc; texturing period, 4 hr, 13 min; argon flow rate, 50 sccm; vacuum chamber pressure, $\sim 1.2 \times 10^{-3}$ Pa (9×10^{-6} torr); temperature (sample receptacle average), 515° C.

Figure 5. – Electron microscope photographs of pyrolytic graphite surfaces examined for electron beam impingement angle effects on secondary electron emission. Angle with surface, 30°.

in texturing parameters noted for these surfaces, but were primarily due to the differences in the original untreated surfaces.

The difference in physical appearance between untreated and ion-textured pyrolytic graphite surfaces is quite marked, as shown by the photograph in figure 6(a). The spire structure formation causes the ion-textured surface to appear optically very dark grey or black. While the surface features of the ion-textured surfaces are readily damaged by abrasion, the spire structures apparently are not damaged by shock and vibration representative of anticipated TWT operating conditions as demonstrated in limited testing at Lewis.

The photograph in figure 6(b) shows an untreated pyrolytic graphite sample disk mounted in the test facility's micromanipulator holding fixture. The bottom half of each sample included in this investigation was cleaned and returned to its untreated condition and coated with soot to provide a control surface. During the evaluation of the sample surface for secondary electron emission characteristics, tests were performed routinely at two or more locations on each half of the disk surface. This procedure helped ensure the validity of the data taken, since the well-known and very repeatable secondary electron emission characteristics of soot provided a standard which would immediately indicate errors in procedure or instrument function should they occur.

Sample Surface Testing

The surfaces studied in this investigation were evaluated for true secondary electron emission and reflected primary electron yield characteristics at eleven primary electron beam energy levels from 200 to 2000 eV for each of eight beam impingement angles from 0° (directly impinging) to 85° (near-grazing). For each angle, the electron gun was focused to produce a spot diameter at the sample of about 10 μm. Tests at identical conditions were repeated routinely and yielded repeatable results (within limits of measurement) in every instance. Scanning electron microscope examinations after lengthy periods of testing revealed no observable surface damage from electron beam impingement for any of the surfaces.

True secondary electron emission. – For the conditions of this investigation, as stated earlier in this report, the total secondary electron emission may be approximated by the true secondary electron emission with the introduction of only a small error. That assumption is made for the purposes of this study.

The following measurements were made to determine true secondary electron emission (see fig. 4). With the selector switch in position 1, the electron gun beam

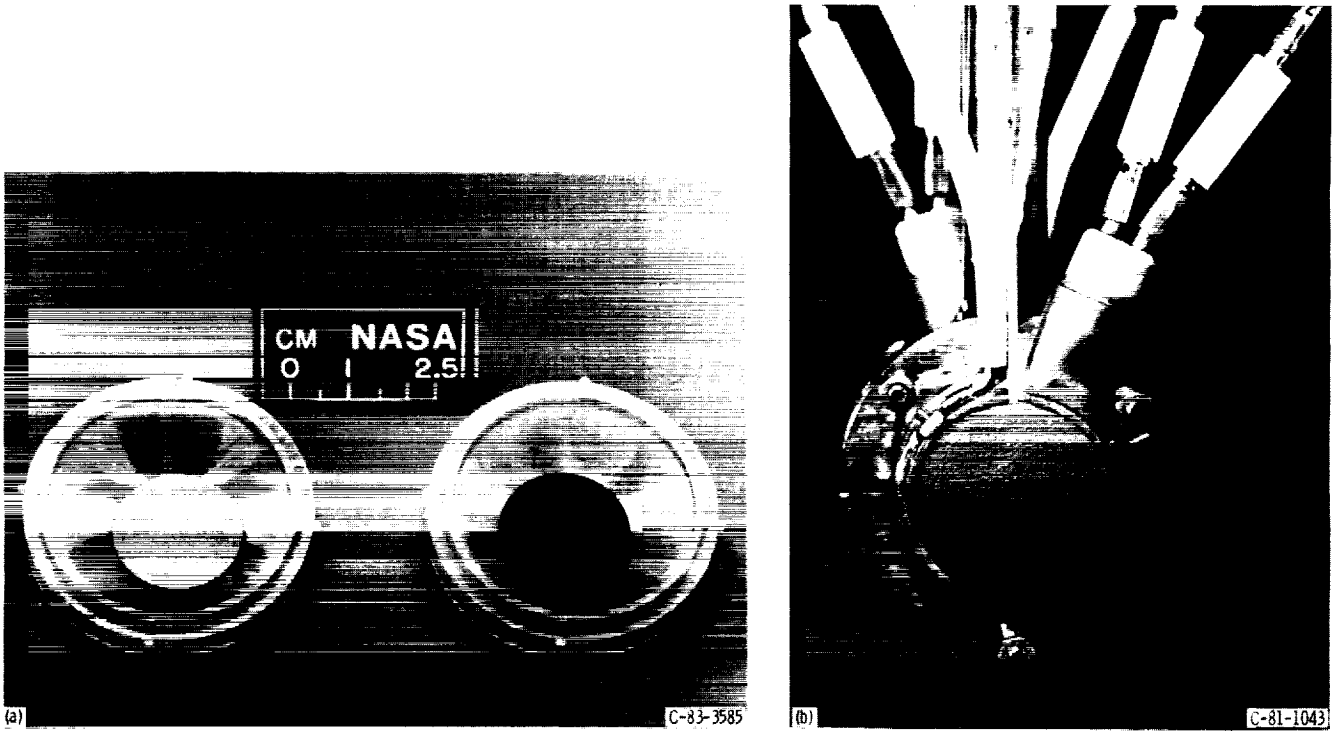

(a) Photograph showing contrast in appearance of untreated (left) and typical ion-textured pyrolytic graphite samples. Samples are shown in storage containers.

(b) Photograph of untreated pyrolytic graphite sample mounted in micromanipulator holding fixture. Note sooted (control surface) bottom half of sample.

Figure 6. – Appearance and positioning of samples for testing.

current minus the secondarily emitted current is indicated by the electrometer in the sample to ground circuit. With the switch in position 2, however, the sample is biased by the 90-V battery and the electrometer indicates the beam current, since now the true secondary electrons are retained by the sample. The secondary electron emission ratio δ or ratio of emitted electrons to primary electrons determined with the use of these measurements is calculated by means of the expression

$$\delta = \frac{I_b - (I_b - I_s)}{I_b}$$

where $I_b - I_s$ is the beam current minus the secondarily emitted current (ranged from about 0.34 to 3.3 μA in this study) and I_b is the beam current (ranged from about 0.48 to 5.3 μA for this study).

The 90-V biasing battery was selected primarily for convenience. While the upper limit for true secondary electron emission is commonly considered to be about 50 V (ref. 7), it was found that for this study only a negligible increase in beam current measurement resulted from using the higher voltage for biasing. For the samples tested, and over the entire primary electron beam energy range studied, the beam current increased by less than 2 percent when the bias voltage was increased from 50 to 90 V, and less than 3 percent when it was increased from 50 to 150 V.

Reflected primary electron yield. – The method for nonquantitatively evaluating the reflected primary electron yield for the surfaces studied in this investigation was adapted from that used in reference 4. The Auger CMA shown schematically in figure 4 is used to analyze the reflected primary yield at each primary electron beam energy level investigated. The amplitudes of the elastic peak curves at each primary energy level are ratioed to the amplitude of the elastic peak curve determined for the soot surface at 1000-eV primary beam energy. If the descriptive plot (as it would be generated by the CMA) of the derivative of reflected electrons relative to primary electron energy presented as part of figure 4 is referred to, it can be seen that, the reflected primary electron yield index π is calculated by

$$\pi_{eV'} = \frac{D_{sample}}{D_{control}}$$

where D_{sample} is the elastic beam curve amplitude for the sample surface at primary electron beam energy eV′ and $D_{control}$ is the elastic curve amplitude for the control surface, soot, at 1000-eV primary electron beam energy.

As has been stated, soot was selected for the control surface (as it was in ref. 4) because of its extremely low secondary electron emission characteristics and its ability to be readily reproduced. While the results of this method of evaluating reflected primary electron yield are nonquantitative, they serve the important purpose of permitting comparison of the properties of different surfaces.

Experimental Results

The experimental results presented in this report are not average or mean values for several identical test conditions but are specific values for one particular test series for each surface examined that is judged to be typical for that surface. A relatively large number of test series were performed during the investigation to form the basis of that judgment. Furthermore, specific test conditions were repeated routinely for each surface at different locations on the surface to assure the validity of the data recorded. Scanning electron microscope examinations were conducted for each surface to assure uniform conditions and reduce the possibility of inadvertantly selecting an unusual or atypical location for testing.

The ion-texturing procedures for the pyrolytic graphite surface examined for this investigation are not necessarily those which produce an optimum surface for secondary electron emission suppression. Rather, the described procedures are those which were being studied when this investigation was begun and which have been shown to result in surfaces whose secondary electron emission characteristics are much lower than those of untreated pyrolytic graphite surfaces.

Sample Surface Auger Examinations

As described earlier, Auger spectrometer examinations of each test surface were performed both before and after the samples were baked out or degassed at 500° C for about 3 hours. Based on the results of a large number of samples that were examined during this investigation, the Auger spectra presented in figure 7 for ion-textured and untreated pyrolytic graphite and sooted surfaces are judged to be typical for both pre- and post-degassing conditions. The surfaces were remarkably free of chemical species other than carbon. The ion-textured surfaces occasionally exhibited some indications of argon (the texturing ion), which was usually but not always entirely removed during the 500° C degassing procedure. The Auger examination for one ion-textured sample indicated some sulfur was present on the surface before degassing but not after the heating procedure. In general, secondary electron emission measurements made before and after the 500° C sample degassing procedure were essentially identical. That was probably due in large part to the unintentional but unavoidable sample degassing

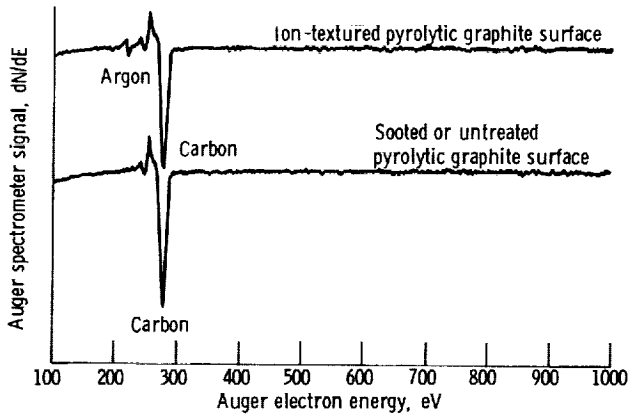

Figure 7. – Typical pre- and post-bakeout Auger spectra for ion-textured pyrolytic graphite and sooted or untreated pyrolytic graphite surfaces.

which occurred during the previously described normal vacuum chamber pumpdown procedure in which the entire chamber was heated to 250° C for 16 hours.

True Secondary Electron Emission Measurements

True secondary electron emission consists of low-energy electrons which reemit from a material surface after undergoing inelastic collisions near the surface of the material. Reference 15 indicates that for carbon the electron mean free path, or the electron penetration distance from the surface, ranges from 4.64 to 23.4 Å for primary electron beam energies of 200 and 2000 eV, respectively. Curves presenting the true secondary electron emission ratio as a function of primary electron beam energy and beam impingement angle for the five sample surfaces examined during this investigation appear in figures 8(a), 9(a), 10(a), 11(a), and 12(a).

For each of the five sample surfaces studied, the true secondary electron emission ratio generally increased with electron beam impingement angle at all points over the primary electron beam energy range examined. That order is not clearly defined for the untreated pyrolytic graphite C surface (figs. 5(d) and 11(a)) at energy levels below about 1000 eV, probably because of the irregular and randomly distributed rough features of its surface. Because of that characteristic, the complex features of the area on which the primary beam impinged changed significantly and irregularly as the impingement angle was changed. The reason for the observed increase in true secondary electron emission with electron beam impingement angle probably differs for the two general classes of surfaces represented in this investigation. The sooted surface (fig. 5(a)) and the untreated pyrolytic graphite AB surface (fig. 5(b)) are relatively smooth with no major projecting features. As the electron beam impingement angle is increased for these smooth surfaces, the impinging electrons penetrate to decreasing

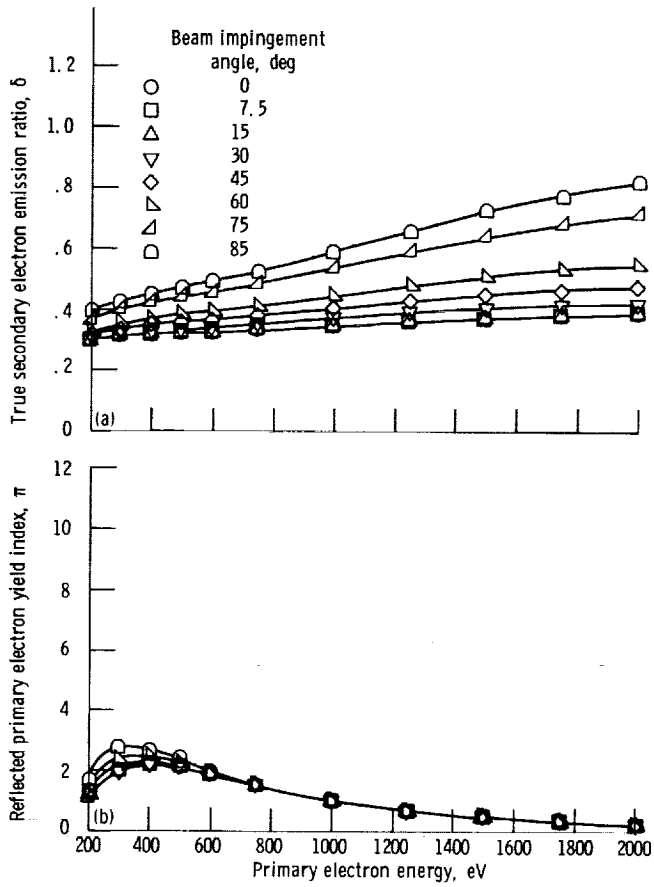

(a) True secondary electron emission ratio as function of primary electron energy.
(b) Reflected primary electron yield index as function of primary electron energy.

Figure 8. – Soot on smooth, untreated pyrolytic graphite AB surface.

distances below the surface levels. The emitted secondary electrons consequently have a shorter distance to travel to escape the surface and therefore escape in increasing numbers as the beam angle increases (figs. 8(a) and 9(a)).

The second general class of sample surfaces examined has significantly distressed characteristics and must be considered differently from the samples with smooth surfaces. The ion-textured AB (fig. 5(c)) and C (fig. 5(e)) surfaces are characterized by closely arrayed, relatively uniform conical spires or peaks. With direct or 0° electron beam impingement angle, most of the electrons strike the sloping conical walls of the spires. The secondary electrons which are emitted are then repeatedly intercepted by nearby adjacent spire walls, thereby reducing the net emission from the projected surface area. As the electron beam impingement angle is increased, the extent of beam penetration into the ion-textured surface is reduced, thereby reducing the electron trapping effect and permitting net true secondary electron emission to increase (figs. 10(a) and 12(a)). The

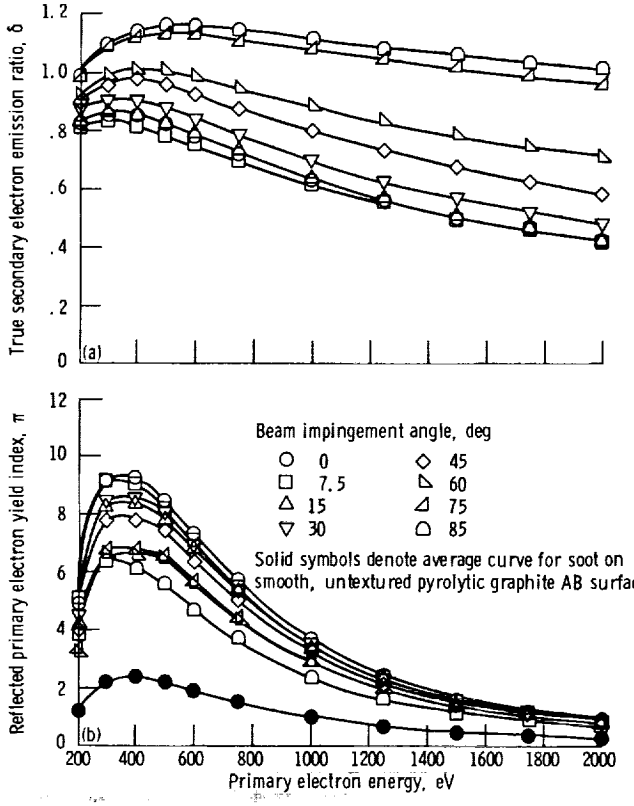

(a) True secondary electron emission ratio as function of primary electron energy.

(b) Reflected primary electron yield index as function of primary electron energy.

Figure 9. – Smooth, untreated pyrolytic graphite, AB surface.

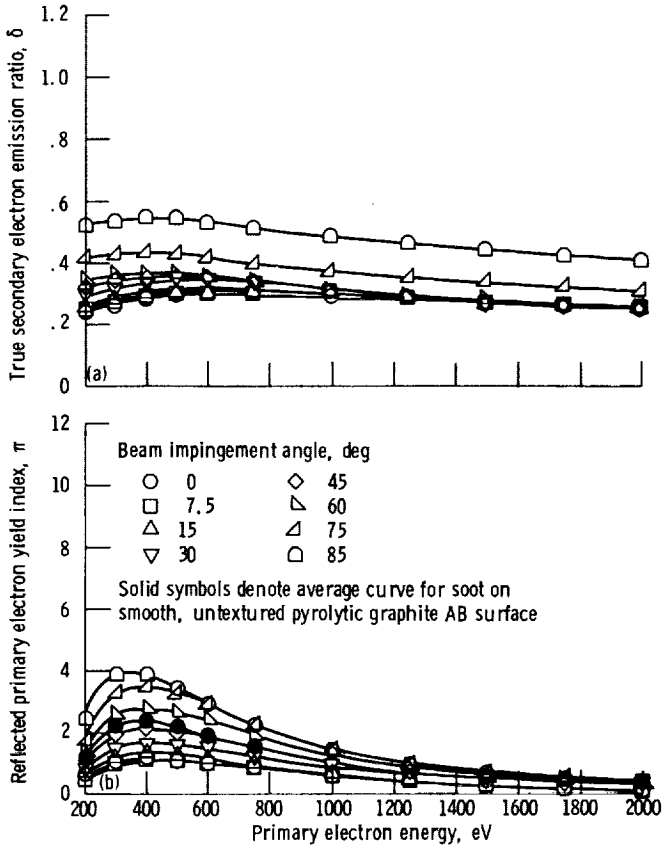

(a) True secondary electron emission ratio as function of primary electron energy.

(b) Reflected primary electron yield index as a function of primary electron energy.

Figure 10. – Ion-textured pyrolytic graphite, AB surface.

untreated pyroloytic graphite C surface (fig. 5(d)), characterized by closely arrayed but nonuniform and relatively shallow crevices and depressions (compared to the ion-textured surfaces), displayed the secondary-emission-reduction tendency to a lesser extent. This surface, because of its relatively smoother surface, displayed a more rapid increase in true secondary electron emission with increasing electron beam impingement angle at primary electron energies above about 1000 eV than did the ion-textured surfaces (fig. 11(a)).

Of the surfaces practical for MDC application (omitting consideration of the sooted control surface), the two ion-textured pyrolytic graphite surfaces clearly display the lowest levels of true secondary electron emission. At small electron beam impingement angles (less than about 60°) and particularly at primary electron beam energies greater than about 600 eV, the two ion-textured surfaces exhibited lower secondary electron emission ratios than the *ideal* control sooted surface (see figs. 8(a), 10(a), and 12(a)). Of these two surfaces, the ion-textured C surface exhibits moderately lower secondary electron emission characteristics than does the ion-textured AB surface.

Reflected Primary Electron Yield Measurements

Curves presenting the reflected primary electron yield index π, which is the reflected primary electron yield relative to that of soot at 1000 eV primary beam energy, as a function of primary electron beam energy and beam impingement angle appear in figures 8(b), 9(b), 10(b), 11(b), and 12(b). Reflected primary electron yield consists of electrons which experience elastic collisions with a surface and reflect at or very near the primary energy level. The primary electron yield measured in this study is only that which is reflected directly at or very nearly directly at the Auger spectrometer CMA and which therefore is the most important from the standpoint of MDC efficiency effects.

The reflected primary electron yield index for the control sooted pyrolytic graphite surface, presented in figure 8(b), is a function only of primary electron beam energy above about 600 eV and is only a moderate and poorly defined function of electron beam impingement angle below that level. Since the sooted surface can be accurately described as one on which a great number of relatively uniformly shaped carbon particles are piled to a

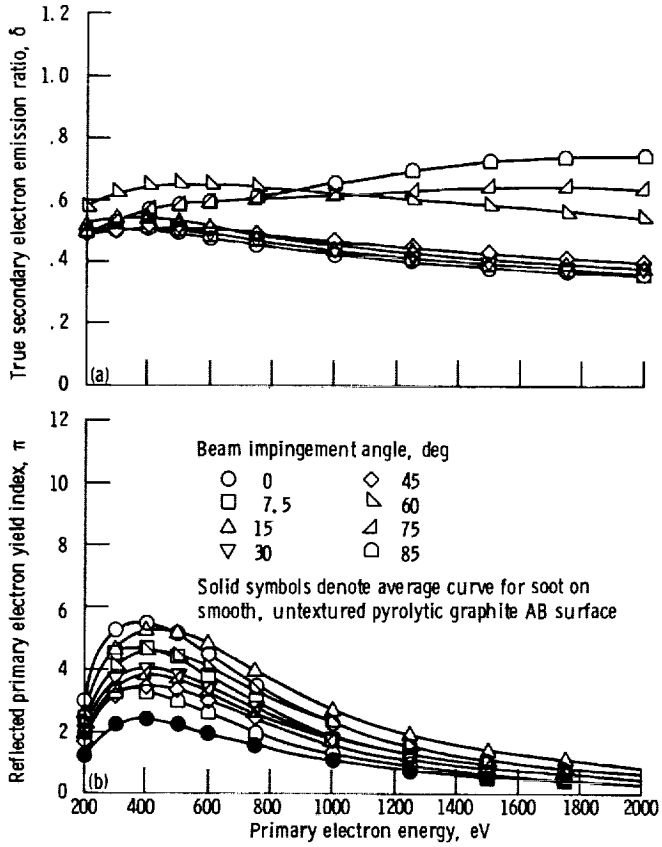

(a) True secondary electron emission ratio as function of primary electron energy.

(b) Reflected primary electron yield index as function of primary electron energy.

Figure 11. – Untreated pyrolytic graphite, C surface.

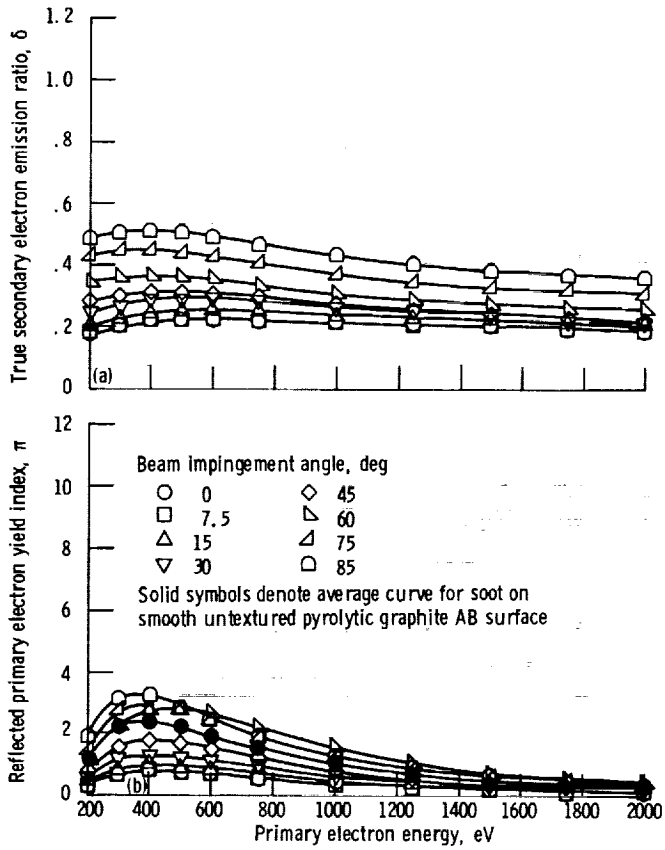

(a) True secondary electron emission ratio as function of primary electron energy.

(b) Reflected primary electron yield index as function of primary electron energy.

Figure 12. – Ion-textured pyrolytic graphite, C surface.

uniform thickness, the surface configuration on which the primary electron beam impinges changes very little with increasing beam impingement angle. As a consequence, the reflected primary electron yield detected by the CMA is relatively constant with beam impingement angle for the electron beam energy range investigated. For comparison of the relative reflected primary electron yield characteristics of soot with those of the other surfaces studied in this investigation, a mean curve was constructed through the data of figure 8(b). This curve appears (with solid circular points) on the corresponding curve sets for the other surfaces (figs. 9(b), 10(b), 11(b), and 12(b)).

The untreated pyrolytic graphite AB and C surfaces (figs. 5(b) and (c), respectively) are relatively smooth compared to the same materials when they are ion-textured. With an increasing primary electron beam impingement angle, the electrons which experience elastic collisions reflect increasingly in directions away from the CMA, resulting in increasingly smaller measurements of reflected primary electron yield. This tendency is evident in figures 9(b) and 11(b) for the untreated pyrolytic graphite AB and C surfaces, respectively. Since the untreated AB surface is much smoother than the randomly and moderately distressed untreated C surface, the effect of reducing measured reflected primary electron yield with increasing electron beam impingement angle is more pronounced with the AB surface. Both of these surfaces display higher relative reflected primary electron yield characteristics than indicated by the mean data line for the sooted surface described earlier and which is plotted (with darkened circular points) on figures 9(b) and 11(b).

Both the ion-textured pyrolytic graphite AB and C surfaces (figs. 5(c) and 5(e), respectively) are characterized by uniformly arrayed conical spires extending at right angles to the sample surface. As the electron beam impingement angle is increased for these surfaces, much of the area on which the beam impinges (the sides of the spires) is rotated so that it increasingly faces the CMA directly. This results in increased measured reflected primary electron yield with increasing impingement angle, as shown in the characteristic π curves for the AB surface (fig. 10(b)) and the C surface

(fig. 12(b)). Each of the two ion-textured surfaces exhibited lower reflected primary electron yield characteristics than the untreated pyrolytic graphite AB and C surfaces examined, and each has superior (lower) characteristics than those of the *ideal* sooted control surface at beam impingement angles less than 45°. Of the two ion-textured pyrolytic graphite surfaces, the C surface displayed moderately lower reflected primary electron yield characteristics.

Conclusions

Ion-textured and untreated pyrolytic graphite surfaces, along with a sooted control surface, were experimentally investigated to determine their true secondary electron emission and relative reflected primary electron yield characteristics. Pyrolytic graphite surfaces both parallel to (AB surface) and normal to (C surface) the planes of material deposition were examined. The surfaces were tested over a range of primary electron beam energies from 200 to 2000 eV and beam impingement angles from direct (0°) to near-grazing angles (85°). This investigation assessed the use of ion-textured pyrolytic graphite as collector elements in multistage depressed collectors (MDC's) for high-efficiency microwave amplifier traveling-wave tubes (TWT's) for space and aircraft applications. To attain high MDC efficiency, the electrode surfaces must have low secondary electron emission characteristics. While soot is not suitable for use in an MDC assembly, it provides a consistently reproducible *ideal* comparison surface because of its extremely low secondary electron emission characteristics.

Both the ion-textured AB and C pyrolytic graphite surfaces exhibited significantly lower true secondary electron emission and relative reflected primary electron yield levels than the same surfaces without texturing (untreated) at all primary electron beam energies and impingement angles investigated. Furthermore, the secondary electron emission characteristics of those ion-textured surfaces compared very favorably with those of the *ideal* sooted control surface used as reference. At all beam impingement angles at electron beam energies above about 600 eV and at all beam energies with impingement angles less than about 60°, both ion-textured surfaces displayed lower true secondary electron emission levels than did those of soot. Also, both ion-textured surfaces exhibited relative primary electron yield levels below those of the sooted surface at all energy levels at electron beam impingement angles up to 45° or slightly higher, with only modest additional increases noted for beam impingement angles up to 85°.

Either of the ion-textured pyrolytic graphite surfaces examined appears to be capable of providing an extremely effective low secondary electron emission material for the MDC electrode application. The ion-textured C surface displayed moderately lower secondary electron emission characteristics than did the ion-textured AB pyrolytic graphite surface.

Lewis Research Center
National Aeronautics and Space Administration
Cleveland, Ohio 44135, November 28, 1983

References

1. Kosmahl, H. G.: A Novel, Axisymmetric, Electrostatic Collector for Linear Beam Microwave Tubes. NASA TN D-6093, 1971.
2. Kosmahl, H. G.; and Ramins, P.: Small-Size 81- to 83.5-Percent Efficient 2- and 4-Stage Depressed Collectors for Octave-Bandwidth High-Performance TWT's. IEEE Trans. Electron Devices, vol. ED-24, Jan. 1977, pp. 36-44.
3. Smith, W. H.; and Leeds, D. H.: Pyrolytic Graphite. Modern Materials-Advances in Development and Applications, B. W. Gonser, ed., vol. 7, Academic Press, 1970.
4. Forman, R.: Secondary-Electron-Emission Properties of Conducting Surfaces With Application to Multistage Depressed Collectors for Microwave Amplifiers. NASA TP-1097, 1977.
5. Wintucky, E. G.; Curren, A. N.; and Sovey, J. S.: Electron Reflection and Secondary Emission Characteristics of Sputter-Textured Pyrolytic Graphite Surfaces. NASA TM-81755, 1981.
6. Dayton, J. A., Jr.; Kosmahl, H. G.; and Ramins, P.: Experimental Verification of the Multistage Depressed Collector Design Procedure for a High-Perveance, Helix-Type, Traveling-Wave Tube. NASA TP-2162, 1983.
7. Beck, Arnold Hugh, ed.: Handbook of Vacuum Physics, Volume 2, Physical Electronics. Pergamon Press, 1966.
8. Kohl, Walter Heinrich: Handbook of Materials and Techniques for Vacuum Devices. Reinhold Publishing Corp., 1967.
9. Walker, Philip L., Jr.; and Thrower, Peter A., eds.: Chemistry and Physics of Carbon; a Series of Advances. Vol. 11. Marcel Dekker, Inc., 1973.
10. Pyrolytic Graphite. Specification 101-B. Revised March 8, 1972. B. F. Goodrich.
11. Pyrolytic Graphite. TR-185-5. Pfizer, Inc., 1973.
12. "PG" Pyrolytic Graphite Grade HPG. Technical Information Bulletin No. 442-212II, Union Carbide Corporation.
13. Curren, A. N.; and Fox, T. A.: Traveling-Wave Tube Efficiency Improvement with Textured Pyrolytic Graphite Multistage Depressed Collector Electrodes. IEEE Electron Device Letters, vol. EDL-2, no. 10, Oct. 1981, pp. 252-254.
14. Sovey, J. S.: Characteristics of a 30-cm Diameter Argon Ion Source-for Ion Thrusters and Sputtering. AIAA Paper 76-1017, Nov. 1976.
15. Penn, David R.: Quantitative Chemical Analysis by ESCA. J. Electron Spectrosc. and Relat. Phenom., vol. 9, no. 1, July 1976, pp. 29-40.

1. Report No.	2. Government Accession No.	3. Recipient's Catalog No.
NASA TP-2285		

4. Title and Subtitle	5. Report Date
Beam Impingement Angle Effects on Secondary Electron Emission Characteristics of Textured Pyrolytic Graphite	February 1984
	6. Performing Organization Code 506-58-22
7. Author(s) Arthur N. Curren and Kenneth A. Jensen	8. Performing Organization Report No. E-1886
	10. Work Unit No.
9. Performing Organization Name and Address National Aeronautics and Space Administration Lewis Research Center Cleveland, Ohio 44135	11. Contract or Grant No.
	13. Type of Report and Period Covered Technical Paper
12. Sponsoring Agency Name and Address National Aeronautics and Space Administration Washington, D.C. 20546	14. Sponsoring Agency Code

15. Supplementary Notes

16. Abstract

Experimentally determined values of true secondary electron emission and relative values of reflected primary electron yield for untreated and ion-textured pyrolytic graphite over a range of primary electron energy levels and electron beam impingement angles are presented. The purpose of the investigation is to provide information required to develop high-efficiency multistage depressed collectors (MDC's) for microwave amplifier traveling-wave tubes for space communication and aircraft applications. To attain the highest possible MDC efficiencies, the electrode surfaces must have low secondary electron emission characteristics. Pyrolytic graphite, a chemically vapor-deposited material, is a particularly promising candidate for this application. The pyrolytic graphite surfaces studied in this investigation were tested over a range of primary electron beam energies and beam impingement angles from 200 to 2000 eV and direct (0°) to near-grazing angles (85°), respectively. Surfaces both parallel to and normal to the planes of material deposition were examined. The true secondary electron emission and reflected primary electron yield characteristics of the pyrolytic graphite surfaces are compared to those of sooted control surfaces. While soot, or carbon black, is not suitable for MDC use, it provides a consistently reproducible "ideal" comparison surface because of its known extremely low secondary electron emission characteristics. The ion-textured pyrolytic graphite surfaces which were studied exhibited extremely low true secondary electron emission and reflected primary electron yield characteristics, even lower than those of the sooted surfaces at small electron beam impingement angles.

17. Key Words (Suggested by Author(s))	18. Distribution Statement
Secondary electron emission Graphite Carbon Traveling-wave tubes Multistage depressed collectors	Unclassified - unlimited STAR Category 27

19. Security Classif. (of this report)	20. Security Classif. (of this page)	21. No. of pages	22. Price*
Unclassified	Unclassified	15	A02

*For sale by the National Technical Information Service, Springfield, Virginia 22161

NASA-Langley, 1984